Human gene therapy for RPE65 isomerase deficiency activates the retinoid cycle of vision but with slow rod kinetics

Artur V. Cideciyan*†, Tomas S. Aleman*, Sanford L. Boye‡, Sharon B. Schwartz*, Shalesh Kaushal‡, Alejandro J. Roman*, Ji-jing Pang‡, Alexander Sumaroka*, Elizabeth A. M. Windsor*, James M. Wilson§, Terence R. Flotte¶, Gerald A. Fishman‖, Elise Heon**, Edwin M. Stone††, Barry J. Byrne‡, Samuel G. Jacobson*, and William W. Hauswirth‡

*Scheie Eye Institute, Department of Ophthalmology and §Department of Pathology and Laboratory Medicine, University of Pennsylvania, Philadelphia, PA 19104; ‡Department of Ophthalmology, University of Florida, Gainesville, FL 32610; ¶University of Massachusetts Medical School, Worcester, MA 01655; ‖Department of Ophthalmology and Visual Sciences, University of Illinois, Chicago, IL 60612; **Department of Ophthalmology and Vision Sciences, Hospital for Sick Children, University of Toronto, Toronto, ON, Canada M5G 1X8; and ††Department of Ophthalmology, University of Iowa Carver College of Medicine, Iowa City, IA 52242

Edited by Jeremy Nathans, Johns Hopkins University School of Medicine, Baltimore, MD, and approved August 6, 2008 (received for review July 21, 2008)

The *RPE65* gene encodes the isomerase of the retinoid cycle, the enzymatic pathway that underlies mammalian vision. Mutations in *RPE65* disrupt the retinoid cycle and cause a congenital human blindness known as Leber congenital amaurosis (LCA). We used adeno-associated virus-2-based *RPE65* gene replacement therapy to treat three young adults with *RPE65*-LCA and measured their vision before and up to 90 days after the intervention. All three patients showed a statistically significant increase in visual sensitivity at 30 days after treatment localized to retinal areas that had received the vector. There were no changes in the effect between 30 and 90 days. Both cone- and rod-photoreceptor-based vision could be demonstrated in treated areas. For cones, there were increases of up to 1.7 log units (i.e., 50 fold); and for rods, there were gains of up to 4.8 log units (i.e., 63,000 fold). To assess what fraction of full vision potential was restored by gene therapy, we related the degree of light sensitivity to the level of remaining photoreceptors within the treatment area. We found that the intervention could overcome nearly all of the loss of light sensitivity resulting from the biochemical blockade. However, this reconstituted retinoid cycle was not completely normal. Resensitization kinetics of the newly treated rods were remarkably slow and required 8 h or more for the attainment of full sensitivity, compared with <1 h in normal eyes. Cone-sensitivity recovery time was rapid. These results demonstrate dramatic, albeit imperfect, recovery of rod- and cone-photoreceptor-based vision after *RPE65* gene therapy.

dark adaptation | photoreceptor | retinal degeneration | retinoid cycle

The enzymatic pathway in the human eye that regenerates light-altered vitamin A molecules is known as the retinoid cycle of vision. Molecular defects in retinoid cycle genes can lead to inherited retinal diseases in man (1). The severity of visual disturbance in these diseases is thought to be related to how the mutation alters the biochemical activity and whether there is redundancy at the multiple biochemical steps of the cycle. A severe form of incurable childhood blindness, Leber congenital amaurosis (LCA), is caused by mutations in *RPE65* (retinal pigment epithelium-specific protein, 65 kDa), the gene in the retinal pigment epithelium (RPE) that encodes the isomerase. This is the only known enzyme that catalyzes isomerization of all-*trans*-retinyl esters to 11-*cis*-vitamin A. In RPE65 deficiency, photoreceptor cells do not regenerate their visual pigment and vision is not sustained. Retinal anatomy also degenerates, but not entirely (2, 3).

RPE65-deficient animals have been characterized, and proof-of-principle studies using recombinant adeno-associated virus (AAV) vector delivery of *RPE65* to RPE cells have described restoration of vision (2, 4–14). These studies provided the impetus for human safety studies of *RPE65* gene replacement (trials NCT00481546, NCT00643747, NCT00516477, and NCT00422721, www.clinicaltrials.gov). Early reports from human retinal gene replacement trials suggest there are no short-term safety concerns and that modest increases in visual function can be found in some of the subjects (15–17).

Key scientific questions were not answered in these recent human studies. It remains unclear whether rod or cone vision, or both, were restored. It is also unknown whether any vision improvement was complete and fully explained by the level of potentially rescuable photoreceptors remaining in the treatment area. To determine if the genetically flawed retinoid cycle could be restored, we used AAV-based *RPE65* gene replacement in three young adult subjects with severe visual loss caused by recessive *RPE65* mutations. Rod and cone visual parameters were studied before and after intervention. Rod photoreceptor-based vision was present in all patients after treatment. Unexpectedly, rod kinetics of dark adaptation, a surrogate for retinoid cycle activity (18), were remarkably slow. Increased cone photoreceptor-based vision was demonstrated in two of the patients. Comparison of photoreceptor nuclear layer structure and co-localized visual function indicated that the intervention had ameliorated the severe retinoid cycle blockade component of this complex disease and converted it to a simpler photoreceptor degeneration.

Results

Human Gene Therapy Surmounts Biochemical Blockade in *RPE65*-LCA. The retinoid cycle enzymatic pathway allows continuous vision by regeneration of 11-*cis*- from all-*trans*-retinal (Fig. 1 *A* and *B*). AAV2-based *RPE65* gene replacement was delivered by injection (5.96×10^{10} vg in 150 μl) between the RPE cell layer and the photoreceptor layer (Fig. 1*C*) into one eye (i.e., study eye) of three *RPE65*-LCA subjects. Subjects' ages were 24 years (patient 1), 23

Author contributions: A.V.C., T.S.A., S.K., T.R.F., B.J.B., S.G.J., and W.W.H. designed research; A.V.C., T.S.A., S.L.B., S.B.S., S.K., A.J.R., J.-j.P., E.A.M.W., G.A.F., E.H., E.M.S., B.J.B., S.G.J., and W.W.H. performed research; A.V.C., S.L.B., J.M.W., S.G.J., and W.W.H. contributed new reagents/analytic tools; A.V.C., T.S.A., S.L.B., S.B.S., A.J.R., A.S., S.G.J., and W.W.H. analyzed data; and A.V.C., S.G.J., and W.W.H. wrote the paper.

Conflict of interest statement: B.J.B., W.W.H., and the University of Florida have a financial interest in the use of AAV therapies and own equity in a company (AGTC Inc.) that might, in the future, commercialize some aspects of this work. J.M.W. is an inventor on patents related to gene therapy that have been licensed to a number of biopharmaceutical companies. University of Pennsylvania, University of Florida, and Cornell University hold a patent on the described gene therapy technology (United States Patent 20070077228, "Method for Treating or Retarding the Development of Blindness").

This article is a PNAS Direct Submission.

†To whom correspondence should be addressed. Email: cideciya@mail.med.upenn.edu.

This article contains supporting information online at www.pnas.org/cgi/content/full/0807027105/DCSupplemental.

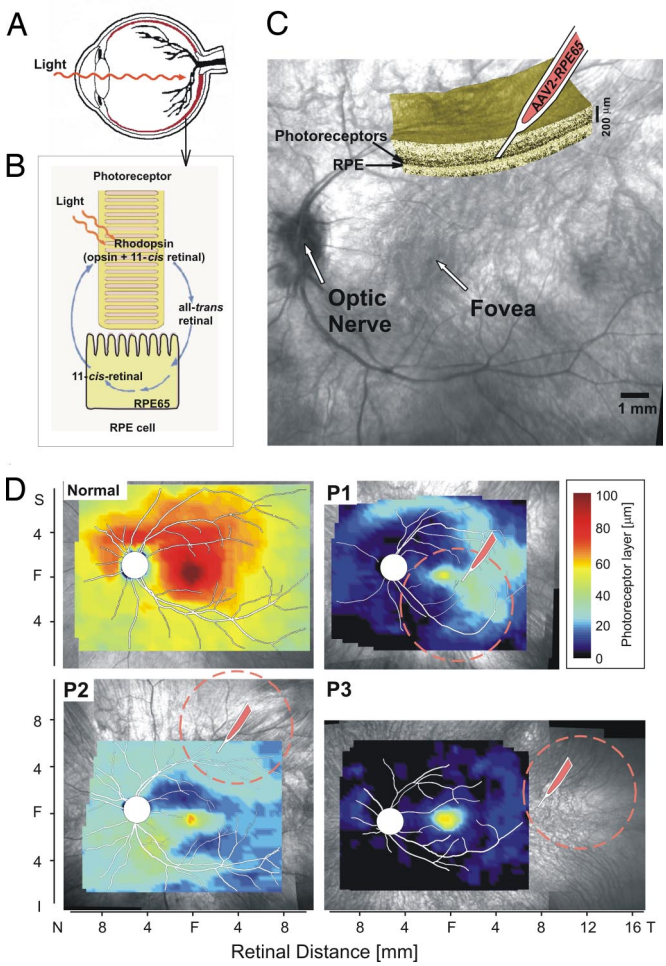

Fig. 1. Schematic of the retina, retinoid cycle, and localized delivery of gene therapy in three patients with inherited blindness. (*A*) Light enters the eye and is absorbed by visual pigments (rhodopsin) in photoreceptors of the retina (red), the complex brain-like neural layer. (*B*) The retinoid cycle and its isomerase, RPE65, converts all-*trans*- to 11-*cis*-retinal to regenerate the visual pigment. (*C*) Series of retinal cross-sections from patient 2 rendered in three dimensions and overlaid onto the ocular fundus view illustrate the superior retinal site of subretinal vector injection. Fovea and optic nerve head locations are shown. (*D*) Photoreceptor cell layer (i.e., ONL) thickness topography (pseudocolor scale) in a normal subject and pretreatment in study eyes of patients 1, 2, and 3 (*P1*, *P2*, and *P3*). Site of injection (syringe tip) and the estimate of the bleb formed by the injection (dashed circle) are shown. Data in *C* and *D* are shown in equivalent left retina representation for clarity.

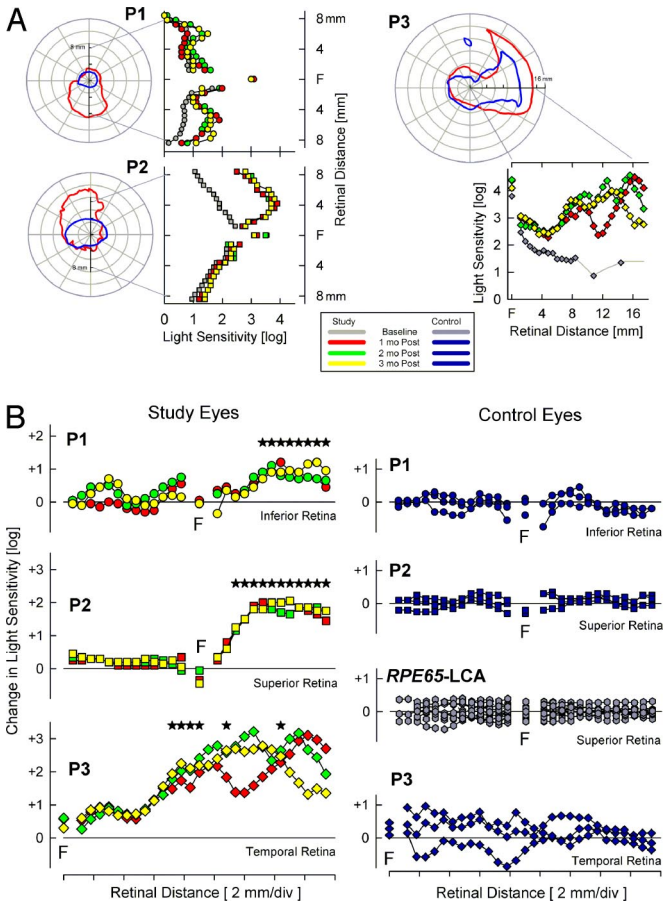

Fig. 2. Biological activity resulting from localized gene therapy in three patients with inherited blindness. (*A*) Clinical kinetic visual field maps (represented as left retina for clarity and comparability) in control (blue) and study eyes at 1 month after treatment (red) are shown. Light sensitivity measures in study eyes along vertical (patients 1 and 2) and horizontal (patient 3) meridians at 1, 2, and 3 months after treatment compared with before treatment are also shown. The increased superior (patient 1), inferior (patient 2), and temporal (patient 3) retinal extent of vision boundary on visual field maps of study eyes corresponds to the region of vector injection. These regions show increases in light sensitivity after treatment compared with before treatment. (*B*) Retinal loci demonstrating significant change (stars) in light sensitivity at 1, 2, and 3 months after treatment compared with before treatment. All significant changes were increases in sensitivity (ranging from 1 to 3 log units) and correspond to regions of study eyes that received gene therapy; control eyes of the three patients did not show significant changes. Test-retest variability estimated from five additional patients with *RPE65*-LCA along the vertical meridian was smaller than the magnitude of sensitivity changes observed in study eyes. Biological activity in the study eye of patient 3 is assumed to cover a large contiguous region even though significance could be mathematically determined only at a subset of far temporal loci where pretreatment sensitivities were available. The baseline for each patient corresponds to the mean of two visits within 20 months of treatment. F, fovea.

years (patient 2) and 21 years (patient 3) and all had severe vision disturbances from childhood. The disease-causing *RPE65* mutations (patient 1, E417Q/E417Q; patient 2, R91W/R44Q; patient 3, Y368H/Y368H) were reported *in vitro* to have less than 3% isomerization activity compared with WT (19, 20). The photoreceptor cell layer thickness in all three patients was reduced but sufficiently detectable to warrant treatment. Treatment involved the inferior retina in patient 1, superior retina in patient 2, and the far temporal retina in patient 3 (Fig. 1*D*). The biological activity of the human vector unused in the treatment syringe was proven with an *in vivo* bioassay in Rpe65-deficient *rd12* mice [supporting information (SI) Fig. S1*A*].

Patient 1 showed increased vertical extent of daylight visual field in the study eye versus the control eye when measured at 30 days after treatment (Fig. 2*A*). There was increased light sensitivity in the treated inferior retina compared with pretreatment results (Fig. 2 *A* and *B*). The effect in patient 1 was present at 1 month as well as 2 and 3 months after treatment; there was no major change in the lateral extent or magnitude of the visual gain during this interval (Fig. 2 *A* and *B*). Retinal loci corresponding to a contiguous region extending more than 4 mm showed statistically significant increases of sensitivity in the study eye; there were no significant changes in the control eye (Fig. 2*B*).

Patient 2 described a localized increase in brightness as early as 7 to 10 days after treatment. This self-reported increase in visual sensitivity posttreatment is earlier than times previously reported in most animal studies (2, 8, 9, 12, 14). Thus, biological activity was studied in *rd12* mice at 10 days after treatment with the clinical trial vector and compared with control injections. Even at this early

posttreatment time, there was a robust electroretinographic response to the vector and no such response from control injections with vehicle (Fig. S1*B*). Daylight visual fields in patient 2 at 30 days after treatment showed increased vertical extent in the study eye compared with the control eye (Fig. 2*A*). Visual thresholds measured in the dark revealed greater light sensitivity in the superior retina, a region included in the injection (Fig. 1*D*). No change in the lateral extent or magnitude of the visual gain was detectable between days 30 and 90 posttreatment (Fig. 2 *A* and *B*). Statistically significant increases covered a contiguous retinal region of more than 6 mm; there were no significant changes in the control eye (Fig. 2*B*). Test–retest variability in other *RPE65*-LCA patients was smaller than the extent of the increases observed in the treated eyes of patients 1 and 2 (Fig. 2*B*).

Patient 3 also reported increased light sensitivity in the study eye at 7 to 10 days after treatment. Daylight visual fields were increased in horizontal extent compared with the control eye at 30 days after treatment (Fig. 2*A*). Visual testing in the dark at loci representing the far temporal retina revealed a wide region with increased sensitivity compared with pretreatment results. The effect was statistically significant, persistent upon re-tests at 60 and 90 days after treatment, and covered a retinal region greater than 10 mm in extent. There were no significant changes in sensitivity in the control eye. Pupillary reactions in the dark (21, 22) also indicated increased light sensitivity in the study eyes of patients 2 and 3; this method showed no detectable change in sensitivity in the study eye of patient 1 or the control eyes of all three patients (Fig. S2).

Extended Dark Adaptation Reveals a Greater Magnitude of Visual Gain After Treatment. Normal human vision becomes more sensitive to light after an instantaneous decrease in ambient illumination—the process is known as dark adaptation. Normally, full dark adaptation can require up to 1 hour for rod photoreceptor-based night vision (18, 23–27); further changes in light sensitivity after 1 hour are insignificant in normal eyes. Accordingly, initial testing in all patients was performed after a standard dark adaptation period of 1 to 2 h. Clues to the inadequacy of this period were suggested from reports by the subjects of noticeably increased brightness in their treated eye when they awoke from sleep in their darkened rooms. To understand the pathophysiology underlying these reports, testing was repeated after allowing adaptation of eyes to darkness for extended periods (3–8 h). Under these conditions, all three patients showed dramatic further gains in the magnitude of their visual sensitivity. Mean gains were 0.9, 1.3, and 0.7 log units within the treated regions of patients 1, 2, and 3, respectively (Fig. 3*A*); untreated retinal regions showed no significant sensitivity changes with extended adaptation (not shown). These results suggested that the kinetics of the reconstituted retinoid cycle in the study eyes may be abnormally slow. Further, spatially non-uniform improvements observed across the treated retina in all patients indicated large differences in the kinetics of dark adaptation may be present.

Adaptation Kinetics for Treated Cones Are Rapid, but Treated Rod Recovery Takes Many Hours. To define the kinetics of dark adaptation in treated retinas and to differentiate rod from cone kinetics, chromatic sensitivities were measured before and after a desensitizing light flash (Fig. 3*B*). In patient 2, two retinal loci within the treated superior retinal region were studied, whereas in patient 3 a single locus was tested in the far temporal retina; patient 1 did not have sufficient visual function to permit reliable testing. Within 1 minute after the flash, visual function was detectable, and it was mediated by the cone system (Fig. 3*B*). Cone-mediated function remained on a plateau (25), essentially unchanged for more than 120 min, compared with the same period lasting only 7 to 9 min in normal eyes. Emergence of rod function defined the end of the cone-plateau phase at ≈2 h for patient 2 at 3.6 mm superior retina and patient 3 at 17 mm temporal retina; patient 2 at 7.2 mm superior retina remained on the cone plateau for ≈4 h (Fig. 3*B*). Rod photoreceptor-

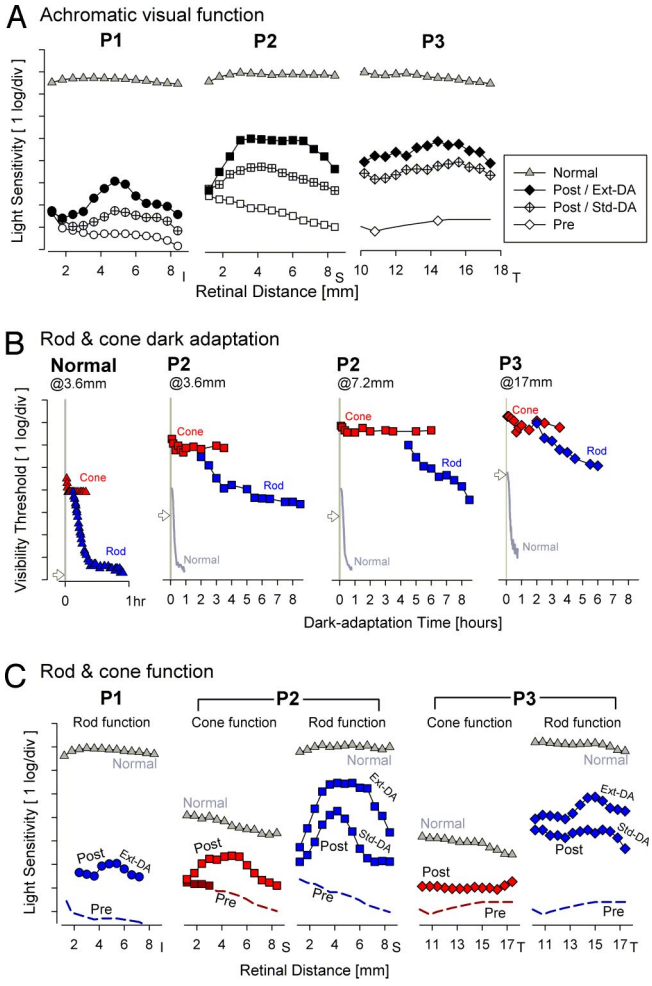

Fig. 3. Rod- and cone-photoreceptor-mediated visual function across the retinal region of study eyes showing biological activity. (*A*) The magnitude of the biological activity can be improved by allowing for a period of extended dark adaptation (Ext DA) before testing. Changes in the shapes of the light sensitivity profiles in patient 1 and patient 2 between standard dark adaptation (StdDA) and extended dark adaptation conditions suggest local differences in adaptation rate. (*B*) Dark adaptation kinetics measured with chromatic stimuli after a 7 log scot-td.s yellow adapting flash (presented at time 0) in patient 2 (at 3.6 and 7.2 mm inferior loci) and patient 3 (at 17 mm temporal locus). Also shown are detailed results from one normal (N) subject at 3.6 mm inferior (*Left*) and mean results from normal subjects at each location (gray lines). Cone adaptation kinetics (red symbols) are fast and do not show a difference from healthy cones. Rod adaptation kinetics (blue symbols) are extremely slow compared with healthy rods, and in patient 2 there is evidence for a large intraretinal difference in recovery rate. Additionally, absolute thresholds of both rod and cone systems are abnormally elevated. Note, the vertical threshold scale is inverted compared to the sensitivity scale in *A* to be consistent with traditional presentations of such data sets. (*C*) Maximal improvement in rod-mediated function (blue) across the region of treated retina ranged from 2.3 log in patient 1, 4.8 log in patient 2, and 4.5 log in patient 3; cone vision improvements (red) range from 1.7 log in patient 2 to 1.2 log in patient 3. Note that pretreatment estimates for rod- or cone-mediated vision (dashed lines) are best-case extrapolations from achromatic sensitivity measures. Only in patient 2 were pretreatment chromatic sensitivities measurable at 1–3 mm superior retina, and these measures were consistent with cone mediation. For patient 1, after treatment, specialized testing with a 4° diameter stimulus centered at 4.8 mm inferior retina suggested rod mediation for the blue stimulus. Pretreatment (Pre) results are from ≈18 to ≈3 months before treatment; posttreatment (Post) results are from 1–3 months after treatment.

mediated recovery in both patients progressed slowly, lasting at least 8 h. The shape of the rod recovery function could be described with two log-linear segments in patient 2 at the 3.6 mm superior locus with slopes of -0.6 h^{-1} and -0.18 h^{-1} (corresponding to time constants of 43 and 145 min); the exact shapes of the other two recovery functions were less discernible but the major log-linear segments had slopes of -0.6 h^{-1}. In normal eyes, rod recovery following a similar flash shows two log-linear segments with slopes of -0.25 min^{-1} and -0.04 min^{-1} (corresponding to time constants of 1.7 and 11 min).

Rod- and Cone-Based Vision Increases After Gene Therapy. Cone function was evaluated across the treated retinal regions of patients 2 and 3 during the extended cone-plateau phase of dark adaptation with chromatic stimuli (Fig. 3*C*). At retinal regions with peak biological activity, cone-mediated sensitivities increased by at least 1.7 log units in patient 2 and 1.2 log units in patient 3 compared with the most conservative (i.e., best-case) estimates of pretreatment cone vision (Fig. 3*C*, red dashed lines). In both patients, cone function posttreatment remained ≈1.5 log units less sensitive than normal. Cone vision in patient 1 was not detectable with the brightest available long-wavelength stimulus (implying a loss of greater than 2.6–3.4 log units, depending on retinal location) before or after treatment.

Under standard dark adaptation conditions, rod-mediated function was discernible after treatment in patients 2 and 3 (Fig. 3*C*) demonstrating 2.3 and 3.1 log units of increased sensitivity on average compared with conservative estimates of pretreatment rod vision (Fig. 3*C*). With an extended period of dark adaptation, rod-mediated function showed further gains of 1.7 log units in patient 2 and 1.0 log unit in patient 3 and became detectable in patient 1 (Fig. 3*C*). The rod function gain observed in patient 2 was not uniform (Fig. 3*C*), consistent with the large intraretinal difference in rate of dark adaptation in this subject (Fig. 3*B*). Posttreatment rod function reached within 1.5 log units of normal vision in patient 2 and within 2.2 log units in patient 3 but remained >4 log units less sensitive than normal in patient 1.

Gene Replacement Converts *RPE65*-LCA from a Complex to a Simpler Disease. *RPE65*-LCA is a complex retinal disease in which visual loss is caused by a combination of a biochemical blockade of the retinoid cycle and degeneration of retinal photoreceptors. In human patients, as well as in canine and murine models, disease stages with partial degeneration of photoreceptors show a dissociation of retinal function from retinal structure whereby the loss of visual function can be orders of magnitude greater than expected from the partial loss of retinal photoreceptors alone (2). Gene replacement therapy would be hypothesized to ameliorate the functional blockade but not replace cells lost as a result of degeneration. To test this hypothesis, we determined the relationship between retinal structure and function in patients 1 and 2 over a ≈2-mm expanse of retina corresponding to each individual's region of peak biological activity (Fig. 4); data on retinal structure could not be obtained within the far temporal locus of patient 3. Photoreceptor layer (outer nuclear layer, ONL) thickness was 29% of mean normal thickness for patient 1 and 43% for patient 2. Patients with retinitis pigmentosa with degenerative photoreceptor loss but without *RPE65* mutations who have ONL thickness values similar to those of patients 1 and 2 showed sensitivity losses ranging from 0.5 to 2.5 log units, consistent (to within measurement variability) with the predictions (0.7–1.1 log units) of a theoretical model (Fig. 4*B*). Pretreatment conservative estimates of the loss of rod function for patients 1 and 2 were 7.2 log and 6.4 log, respectively. After treatment, patient 1 showed a 2.3 log unit increase in rod sensitivity, which approached, but did not reach, the predictions of the simple photoreceptor degeneration (Fig. 4*B*). Patient 2, conversely, showed a posttreatment visual gain of 4.8 log units (i.e., 63,000 fold) and the result became no different from that expected of simpler

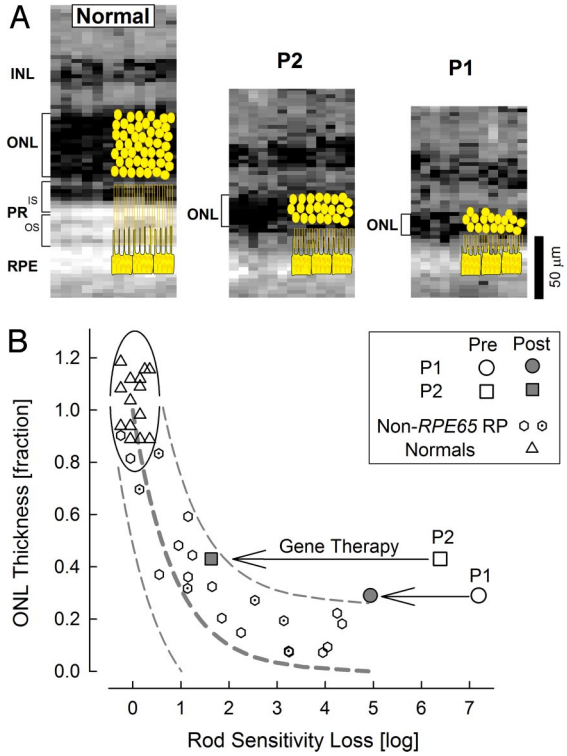

Fig. 4. Pathophysiology of complex visual loss resulting from photoreceptor degeneration and biochemical blockade, and the effect of gene therapy. (*A*) Retinal cross-sectional images at the region of maximal biological activity show the photoreceptor layer (ONL, brackets) to be abnormally thinned; greater degeneration of photoreceptors is evident in patient 1 compared with patient 2. Normal retina and patient 2 are at ≈5 mm superior retina, patient 1 is at ≈5 mm inferior retina. Schematics of photoreceptors and RPE are overlaid (yellow) and to the right of the actual optical images; these are derived from cynomolgus monkey histology (3, 28). INL, inner nuclear layer; PR-IS and PR-OS, photoreceptor inner and outer segments. (*B*) The relationship between photoreceptor layer thickness and rod sensitivity loss in patients 1 and 2 before and after therapy compared with normal subjects and patients with retinitis pigmentosa without mutations in the *RPE65* gene. Normal variability is described by the ellipse encircling the 95% C.I. of a bivariate Gaussian distribution. Dotted lines define the idealized model of the relationship between structure and function in pure photoreceptor degenerations and the region of uncertainty that results from translating the normal variability along the idealized model. Gene therapy (arrows) results in partial (patient 1) or a nearly complete (patient 2) amelioration of the biochemical blockade transforming the complex *RPE65*-LCA disease phenotype into a simpler retinal degeneration phenotype.

diseases with only a degenerative component contributing to the vision loss (Fig. 4*B*). Thus, gene therapy shows the potential to provide dramatic, albeit imperfect, restoration of the retinoid cycle disease component in *RPE65*-LCA.

Discussion

Clinical trials of uniocular subretinal gene therapy in patients with *RPE65*-LCA were initiated after proof-of-concept studies using subretinal delivery of vector gene showed restored vision in Rpe65-deficient dogs (4, 5, 8, 11, 12) and mice (2, 6, 7, 9, 10, 13, 29, 30). Short-term safety results from three human clinical trials were recently reported: there were no serious adverse events in all subjects, and vision improved in some subjects (15–17). In the current study, we explored in detail the basis of increased vision resulting from the intervention.

Rod photoreceptor-based night vision increased in sensitivity in all three subjects who underwent gene therapy in this study. The increase in rod sensitivity was localized to the retinal regions exposed to the therapy. The magnitude of the increase differed

among subjects, and those with a better preserved photoreceptor layer in the treated region showed the greater increases in rod vision. These psychophysical results, complimented by objective evidence from dark-adapted pupillary reflexes, were consistent with our previous demonstration that visual pathways from retina to visual brain were intact and amenable to therapy despite the congenital defect of *RPE65*-LCA (22). The increased rod sensitivity is likely driven by an increased synthesis of 11-*cis*-retinal chromophore resulting from WT RPE65 protein introduced into the RPE by expression from the AAV2 gene therapy vector. These results in man add to the literature consensus that RPE65 is essential in the regeneration of rod visual pigment (i.e., rhodopsin) in vertebrates (1, 19, 31, 32). Both the magnitude of the increase observed (up to 4.8 $\log_{10}$ units) in the human subjects and the lack of visual function increase found with sham subretinal injections in murine (Fig. S1) and canine (11) models with Rpe65 deficiency essentially rule out alternative hypotheses for visual gain involving the release of neurotrophic factors (33) secondary to subretinal surgery (34).

Extremely prolonged recovery of rod vision after light exposure, demonstrated by dark adaptation testing posttreatment in patients 2 and 3 (Fig. 3*B*), suggests a slowed delivery of 11-*cis*-retinal chromophore from the RPE to the rod photoreceptors and thus a protracted regeneration of light responsive rhodopsin. Two general hypotheses to entertain for a slowing of the chromophore delivery rate are (*i*) reduced rate of its synthesis or (*ii*) increased obstruction to its inter- or intracellular transport. Abnormally low expression of RPE65 (or other key retinoid cycle enzymes, ref. 35) could have reduced the rate of chromophore synthesis and resulted in an enzymatic limit to rhodopsin regeneration such as observed in mice that express very low levels of WT Rpe65 (36, 37) or a mutant Rpe65 protein (38). In previous studies, slowness of recovery of rod vision in human diseases of the RPE (23–27) has been ascribed to enzymatic limitation to the synthesis of chromophore (18). A limited expression of RPE65 through gene therapy could have caused such an enzymatic bottleneck. Unlike in disease states, however, the normal human rhodopsin regeneration rate is believed not to be enzymatically limited (18). Consistent with this hypothesis is the demonstration of normal rate of dark adaptation in heterozygotes for null mutations in *RPE65* (39) and *RDH5* (25) predicted to express half the normal amount for the two key retinoid cycle enzymes, the isomerase and the 11-*cis*-retinol dehydrogenase, respectively. As an alternative to an enzymatic limit, the major component of dark adaptation in normal human vision is hypothesized to be rate-limited by a "resistive barrier" to 11-*cis*-retinal diffusion or transport between RPE cells and rod photoreceptors (18). The identity of the resistive barrier is currently unknown, and it is possible that RPE65 disease exacerbates or adds to a natural barrier. The dramatic accumulation of all-*trans*-retinyl esters and lipid droplets observed in the RPE with RPE65 deficiency and/or disorganized rod outer segments may contribute to such a barrier (4, 9, 40, 41). Alternatively, the surgical detachment could have altered the RPE/photoreceptor interface (42). Follow-up studies in the current patients and other patients with similar or higher doses of vector-*RPE65* should help clarify the underlying cause of slowed rod kinetics by considering dose and disease stage dependence of the recovery rate as well as possible changes in dark adaptation rate with time after treatment.

Arguably, cone photoreceptor-based daylight vision is used more than night vision by people living in modern well-lit environments. The role(s) played by RPE65 in providing chromophore for cone function and/or survival remains unclear and controversial (1, 3, 40, 43–49). Restoration of cone- as well as rod photoreceptor-based visual function by subretinal AAV gene therapy in the canine model of RPE65-LCA (4, 8), together with the existence of remnant cone function in patients with untreated *RPE65*-LCA (3), suggested a potential to improve cone function in patients undergoing gene therapy. Indeed, in two of the patients in the current study (patients 2 and 3), robust improvement in cone-mediated visual function could be demonstrated (Fig. 3*C*). In the patient with the best treatment response (patient 2), both cones and rods reached a level of sensitivity within ≈1.5 log units of mean normal. Fast recovery rate of cone dark adaptation function could be attributed to the long-standing hypothesis of rod/cone competition, with cones extracting more of an extremely limited supply of 11-*cis*-retinal chromophore (50). However, alternative hypotheses involving a partial reconstitution of a cone-specific retinoid cycle by gene therapy cannot be ruled out.

How do the present results compare with other similarly conducted *RPE65*-LCA gene therapy trials? Maguire *et al.* (16) reported increased visual acuity after treatment, but these increases were from severely low levels of spatial vision to levels that were still low; extrafoveal rods or cones could have subserved the posttreatment levels of visual acuity reported. Improvement of vision in dim light was self-reported by all three subjects (16) but the photoreceptor cell type subserving this vision was not characterized. Bainbridge *et al.* (15) used dark-adapted thresholds and found as much as 2 log units of increased vision in one patient, but again the photoreceptor type mediating the improvement remained unclear (15). The need to experimentally dissect rod- from cone-mediated responses in our patients suggests that the source of visual improvement with therapy cannot be presumed but must be measured. Of note, none of our patients showed a decrease in nystagmus (Fig. S3), contrary to an observation made in another trial (16). Contributing to this discrepancy could be the large baseline differences in visual acuity between the treatment cohorts; we have previously shown fixation instability to be related to visual acuity in *RPE65*-LCA (3), and treatment of patients with severe loss of central vision as in Maguire *et al.* (16) could conceivably have different consequences on eye movement abnormalities.

There are some key practical implications of the finding of slow rod kinetics after treatment. Clinical trial protocols may need reconsideration as this therapy advances beyond early stages. It is evident that the maximum increase of vision after treatment cannot be measured unless patients undergo dark adaptation for extended periods of time. Comparisons of visual function improvement between patients within a trial or between trials cannot be made without rigorous attention to previous light exposure and length of dark adaptation. The order of testing protocols will need careful reconsideration. In particular, light exposures, such as fundus photography, preceding measures of dark-adapted sensitivities should be minimized. If monitoring the kinetics of adaptation becomes an assay for treatment efficacy, an efficient method should be devised, considering the lengthy time course we observed in two patients.

Materials and Methods

Human Studies. Vision research studies were performed in eight patients with LCA caused by mutations in the *RPE65* gene and conducted according to guidelines of the Declaration of Helsinki after obtaining written consent. All studies were approved by the University of Pennsylvania Institutional Review Board (nos. 186900, 701705, 700942, and 804582). Three of the patients were assessed with these vision research studies before and after taking part in a phase I clinical trial (trial NCT00481546, www.clinicaltrials.gov) evaluating the safety of rAAV2-CB^{SB}-h*RPE65* (IND Number, BB-IND 12824). Safety results of this clinical trial are published separately (17).

Photoreceptor Layer Topography. *In vivo* microscopy of the human retina was performed with optical coherence tomography (OCT) as published (2, 3, 51). A Fourier-domain OCT system (RTVue-100; Optovue) was used for data acquisition, and postacquisition processing of data was performed with custom programs (MatLab 6.5; MathWorks). Further details are described in the *SI Text*.

Psychophysical Studies. Visual field testing was performed with kinetic and static perimetry as published (3, 23–27, 52). For kinetic perimetry, white (318 cd·m^{-2}) targets of Goldmann sizes III (patient 1) or V (patients 2 and 3) were used on a 10

cd·m^{-2} achromatic background. Fixation location and stability were quantified (as described in *SI Text*) in all subjects studied. All subjects fixated at the anatomical fovea; variability of the excursions from the fovea resulting from abnormal eye movements was much smaller than the 0.6-mm sampling density used in static perimetry (Fig. S3). In all three patients, there were no consistent changes in fixation location or fixation instability before and after treatment (Fig. S3). Static perimetric sensitivities were determined with a modified computerized perimeter (Humphrey Field Analyzer; Zeiss) under dark-adapted conditions (see *SI Text* for details).

Modeling of the Relationship Between Retinal Structure and Visual Function. The relationship between photoreceptor structure and co-localized visual function was defined in patients using ONL thickness and rod-mediated sensitivity. Patient results were compared with an idealized model of the expected relationship for ''simple'' photoreceptor degenerations in which vision loss is thought to be derived primarily from degenerative photoreceptor cell loss. The model assumes that absolute sensitivity of rod-mediated function near the visibility threshold is limited by quantum catch and is thus proportional to the product of the number of surviving photoreceptor cells and the length of their outer segments; both of these parameters are proportional to ONL thickness (2, 53, 54). Thus, to a first approximation, loss of light sensitivity (in linear units) would be expected to be proportional to the square of ONL thinning.

Animal Studies. *Rpe65*-deficient *rd12* mice were injected subretinally with 4×10^8 vector genomes of rAAV2-CB^{SB}-h*RPE65*, which remained after each human surgery. Electroretinograms obtained in vector-injected and control eyes were used to determine the biological activity of the vector (13). Further details are described in the *SI Text*.

ACKNOWLEDGMENTS. This work was supported by National Eye Institute (National Institutes of Health, Department of Health and Human Services) Grants U10 EY017280, U10 EY013729, R01 EY011123, R01 EY013385, and P30 EY008571. Additional support was provided by Macula Vision Research Foundation; Foundation Fighting Blindness; Research to Prevent Blindness; and Hope for Vision.

1. Travis GH, Golczak M, Moise AR, Palczewski K (2007) Diseases caused by defects in the visual cycle: retinoids as potential therapeutic agents. *Annu Rev Pharmacol Toxicol* 47:469–512.
2. Jacobson SG, *et al.* (2005) Identifying photoreceptors in blind eyes caused by RPE65 mutations: prerequisite for human gene therapy success. *Proc Natl Acad Sci USA* 102:6177–6182.
3. Jacobson SG, *et al.* (2007) Human cone photoreceptor dependence on RPE65 isomerase. *Proc Natl Acad Sci USA* 104:15123–15128.
4. Acland GM, *et al.* (2001) Gene therapy restores vision in a canine model of childhood blindness. *Nat Genet* 28:92–95.
5. Narfström K, *et al.* (2003) Functional and structural recovery of the retina after gene therapy in the *RPE65* null mutation dog. *Invest Ophthalmol Vis Sci* 44:1663–1672.
6. Dejneka NS, *et al. (2004)* In utero gene therapy rescues vision in a murine model of congenital blindness. *Mol Ther* 9:182–188.
7. Lai C, *et al.* (2004) Recombinant adeno-associated virus type 2-mediated gene delivery into the Rpe65-/- knockout mouse eye results in limited rescue *Genet Vaccines Ther* 2:3.
8. Acland GM, *et al.* (2005) Long-term restoration of rod and cone vision by single dose rAAV-mediated gene transfer to the retina in a canine model of childhood blindness. *Mol Ther* 12:1072–1082.
9. Pang JJ, *et al.* (2006) Gene therapy restores vision-dependent behavior as well as retinal structure and function in a mouse model of RPE65 Leber congenital amaurosis. *Mol Ther* 13:565–572.
10. Chen Y, Moiseyev G, Takahashi Y, Ma JX (2006) RPE65 gene delivery restores isomerohydrolase activity and prevents early cone loss in. Rpe65-/- mice. *Invest Ophthalmol Vis Sci* 47:1177–1184.
11. Jacobson SG, *et al.* (2006) Safety of recombinant adeno-associated virus type 2-*RPE65* vector delivered by ocular subretinal injection. *Mol Ther* 13:1074–1084.
12. Le Meur G, *et al.* (2007) Restoration of vision in *RPE65*-deficient Briard dogs using an AAV serotype 4 vector that specifically targets the retinal pigmented epithelium. *Gene Ther* 14:292–303.
13. Roman AJ, *et al.* (2007) Electroretinographic analyses of Rpe65-mutant rd12 mice: developing an in vivo bioassay for human gene therapy trials of Leber congenital amaurosis. *Mol Vis* 13:1701–1710.
14. Bennicelli J, *et al.* (2008) Reversal of blindness in animal models of Leber congenital amaurosis using optimized AAV2-mediated gene transfer. *Mol Ther* 16:458–465.
15. Bainbridge JW, *et al.* (2008) Effect of gene therapy on visual function in Leber's congenital amaurosis. *N Engl J Med* 358:2231–2239.
16. Maguire AM, *et al.* (2008) Safety and efficacy of gene transfer for Leber's congenital amaurosis. *N Engl J Med* 358:2240–2248.
17. Hauswirth WW, *et al.* (2008) Phase I trial of Leber congenital amaurosis due to *RPE65* mutations by ocular subretinal injection of adeno-associated virus gene vector: Short-term results. *Hum Gene Ther*, in press.
18. Lamb TD, Pugh EN Jr (2006) Phototransduction, dark adaptation, and rhodopsin regeneration. The Proctor lecture. *Invest Ophthalmol Vis Sci* 47:5137–5152.
19. Redmond TM, *et al.* (2005) Mutation in key residues of RPE65 abolishes its enzymatic role as isomerohydrolase in the visual cycle. *Proc Natl Acad Sci USA* 102:13658–13663.
20. Takahashi Y, Chen Y, Moiseyev G, Ma JX (2006) Two point mutations of RPE65 from patients with retinal dystrophies decrease the stability of RPE65 protein and abolish its isomerohydrolase activity. *J Biol Chem* 281:21820–21826.
21. Aleman TS, *et al.* (2004) Impairment of the transient pupillary light reflex in Rpe65-/- mice and humans with Leber congenital amaurosis. *Invest Ophthalmol Vis Sci* 45:1259–1271.
22. Aguirre GK, *et al.* (2007) Canine and human visual cortex intact and responsive despite early retinal blindness from RPE65 mutation. *PLoS Med* 4:e230.
23. Jacobson SG, *et al.* (1995) Night blindness in Sorsby's fundus dystrophy reversed by vitamin A. *Nat Genet* 11:27–32.
24. Cideciyan AV, Pugh EN Jr, Lamb TD, Huang Y, Jacobson SG (1997) Rod plateaux during dark adaptation in Sorsby's fundus dystrophy and vitamin A deficiency. *Invest Ophthalmol Vis Sci* 38:1786–1794.
25. Cideciyan AV, *et al.* (2000) Rod and cone visual cycle consequences of a null mutation in the 11-cis-retinol dehydrogenase gene in man. *Vis Neurosci* 17:667–678.
26. Jacobson SG, Cideciyan AV, Wright E, Wright AF (2001) Phenotypic marker for early disease detection in dominant late-onset retinal degeneration. *Invest Ophthalmol Vis Sci* 42:1882–1890.
27. Cideciyan AV, *et al.* (2004) Mutations in. ABCA4 result in accumulation of lipofuscin before slowing of the retinoid cycle: a reappraisal of the human disease sequence. *Hum Mol Genet* 13:525–534.
28. Jacobson SG, *et al.* (2006) Safety in nonhuman primates of ocular AAV2-RPE65, a candidate treatment for blindness in Leber congenital amaurosis. *Hum Gene Ther* 17:845–858.
29. Bemelmans AP, *et al.* (2006) Lentiviral gene transfer of RPE65 rescues survival and function of cones in a mouse model of Leber congenital amaurosis. *PLoS Med* 3:e347.
30. Yanez-Munoz RJ, *et al.* (2006) Effective gene therapy with nonintegrating lentiviral vectors. *Nat Med* 12:348–353.
31. Jin M, Li S, Moghrabi WN, Sun H, Travis GH (2005) Rpe65 is the retinoid isomerase in bovine retinal pigment epithelium. *Cell* 122:449–459.
32. Moiseyev G, Chen Y, Takahashi Y, Wu BX, Ma JX (2005) RPE65 is the isomerohydrolase in the retinoid visual cycle. *Proc Natl Acad Sci USA* 102:12413–12418.
33. Wen R, *et al.* (1995) Injury-induced upregulation of bFGF and CNTF mRNAs in the rat retina. *J Neurosci* 15:7377–7385.
34. Del Priore LV (2005) Effect of sham surgery on retinal function after subretinal transplantation of the artificial silicone retina. *Arch Ophthalmol* 123:1156.
35. Saari JC, *et al.* (2001) Visual cycle impairment in cellular retinaldehyde binding protein (CRALBP) knockout mice results in delayed dark adaptation. *Neuron* 29:739–748.
36. Wenzel A, Reme CE, Williams TP, Hafezi F, Grimm C (2001) The Rpe65 Leu450Met variation increases retinal resistance against light-induced degeneration by slowing rhodopsin regeneration. *J Neurosci* 21:53–58.
37. Lyubarsky AL, *et al.* (2005) Mole quantity of RPE65 and its productivity in the generation of 11-*cis*-retinal from retinyl esters in the living mouse eye. *Biochemistry* 44:9880–9888.
38. Samardzija M, *et al.* (2008) R91W mutation in Rpe65 leads to milder early-onset retinal dystrophy due to the generation of low levels of 11-*cis*-retinal. *Hum Mol Genet* 17:281–292.
39. Poehner WJ, *et al.* (2000) A homozygous deletion in RPE65 in a small Sardinian family with autosomal recessive retinal dystrophy. *Mol Vis* 6:192–198.
40. Redmond TM, *et al.* (1998) Rpe65 is necessary for production of 11-*cis*-vitamin A in the retinal visual cycle. *Nat Genet* 20:344–351.
41. Porto FB, *et al.* (2002) Prenatal human ocular degeneration occurs in Leber's congenital amaurosis (LCA2). *J Gene Med* 4:390–396.
42. Geller SF, Lewis GP, Fisher SK (2001) FGFR1, signaling, and AP-1 expression after retinal detachment: reactive Müller and RPE cells. *Invest Ophthalmol Vis Sci* 42:1363–1369.
43. Seeliger MW, *et al.* (2001) New views on RPE65 deficiency: the rod system is the source of vision in a mouse model of Leber congenital amaurosis. *Nat Genet* 29:70–74.
44. Znoiko SL, Crouch RK, Moiseyev G, Ma JX (2002) Identification of the RPE65 protein in mammalian cone photoreceptors. *Invest Ophthalmol Vis Sci* 43:1604–1609.
45. Hemati N, *et al.* (2005) RPE65 surface epitopes, protein interactions, and expression in rod- and cone-dominant species. *Mol Vis* 11:1151–1165.
46. Schonthaler HB, *et al.* (2007) Evidence for RPE65-independent vision in the cone-dominated zebrafish retina. *Eur J Neurosci* 26:1940–1949.
47. Zhang H, *et al.* (2008) Trafficking of membrane-associated proteins to cone photoreceptor outer segments requires the chromophore 11-*cis*-retinal. *J Neurosci* 28:4008–4014.
48. Feathers KL, *et al.* (2008) Nrl-knockout mice deficient in Rpe65 fail to synthesize 11-*cis* retinal and cone outer segments. *Invest Ophthalmol Vis Sci* 49:1126–1135.
49. Collery R, *et al.* (2008) Duplication and divergence of zebrafish *CRALBP* genes uncovers a novel role for RPE- and Mueller-*CRALBP* in cone vision. *Invest Ophthalmol Vis Sci* 49:3812–3820.
50. Rushton WA (1968) Rod/cone rivalry in pigment regeneration. *J Physiol* 198:219–236.
51. Jacobson SG, *et al.* (2008) Photoreceptor layer topography in children with Leber congenital amaurosis caused by *RPE65* mutations. *Invest Ophthalmol Vis Sci*, in press
52. Jacobson SG, Yagasaki K, Feuer W, Roman AJ (1989) Interocular asymmetry of visual function in heterozygotes of X-linked retinitis pigmentosa. *Exp Eye Res* 48:670–691.
53. Rohrer B, *et al.* (2003) Correlation of regenerable opsin with rod ERG signal in Rpe65-/- mice during development and aging. *Invest Ophthalmol Vis Sci* 44:310–315.
54. Jacobson SG, *et al.* (2007) RDH12 and RPE65, visual cycle genes causing Leber congenital amaurosis, differ in disease expression. *Invest Ophthalmol Vis Sci* 48:332–338.

Supporting Information

Cideciyan *et al.* 10.1073/pnas.0807027105

SI Text

Photoreceptor Layer Topography. Optical coherence tomography scans were obtained with an ultra-high speed (26,000 A-scans per second) and high-resolution (5 μm axial, 15 μm lateral) Fourier-domain system (RTVue-100; Optovue). Two scanning patterns were used: line scans (4096 A-scans covering 4.5 mm) and raster scans (101 raster lines of 512 A-scans each covering 6 × 6 mm). Multiple overlapping line scans were used to obtain higher-resolution coverage along horizontal and vertical meridians up to 9 mm eccentricity from the fovea (1–4). Similarly multiple overlapping raster scans were used to sample an 18 × 12 mm rectangular region of the retina centered on the fovea (3, 5, 6). Postacquisition processing of data was performed with custom programs (MatLab 6.5; MathWorks). Lateral sampling density of the line scans were reduced by averaging groups of eight neighboring A-scans to increase signal-to-noise ratio, aligned using a dynamic cross-correlation algorithm (7), and digitally stitched along the horizontal and vertical meridians. Two nuclear layers, the ONL and the inner nuclear layer, were defined in regions of scans showing two parallel stereotypical hyporeflective layers sandwiched between the RPE and vitreoretinal interface, and extended laterally to regions with thinner ONL. The boundary of the outer hyporeflective layer corresponding to the ONL was defined by the minima/maxima of the signal slope. For topographic analysis, original raster sets were sub-sampled down to 21 lines after discarding artefactual lines corresponding to blinks and eye movements. The precise location and orientation of each raster line was determined relative to retinal features using video images of the fundus. A-scans were allotted to regularly spaced bins (0.3 × 0.3 mm) in a rectangular coordinate system centered at the fovea; the waveforms in each bin were aligned and averaged. ONL thickness was measured from averaged A-scans in each bin as described earlier. Missing data were interpolated bi-linearly, thickness values were mapped to a pseudocolor scale, and locations of blood vessels and optic nerve head were overlaid for reference.

Psychophysical Studies. Absolute visual sensitivity to stimuli under dark-adapted conditions was determined with a modified computerized perimeter (Humphrey Field Analyzer; Zeiss Meditec) as published (1, 8–11). The achromatic (white) stimulus was 1.7° in diameter and 200 ms in duration (maximum luminance, 3,180 cd·m^{-2}), presented along the vertical or horizontal meridians crossing fixation. Tests were performed at several pretreatment time points ranging from 3 to 24 months before surgery and at three posttreatment time points of day 30, 60, and 90. Retinal loci were typically sampled at 0.6 mm intervals up to 9 (vertical) or 18 (horizontal) mm eccentricity from the fixation. All extrafoveal loci were tested using a red fixation target with a variable intensity adjusted to be visible for each subject. Foveal sensitivities were determined while gazing at the center of four red lights forming a diamond. Sensitivity values were spatially smoothed using a three-point moving average; foveal sensitivities were reported without spatial averaging. Locus-by-locus differences were calculated between posttreatment and pretreatment results. The statistical significance of the difference calculated at each locus was defined by comparison to the maximum expected test–retest variability. To obtain the most conservative estimates, the best pretreatment sensitivity was used for defining loci with significant improvement and the worst pretreatment sensitivity was used for defining loci with significant deterioration. The maximum expected test–retest variability limit (3 SD = 0.80 log units) was based on the range of sensitivities obtained in patients with *RPE65*-LCA (n = 8) who were each tested two or three times on consecutive days. For the variability estimates, if data were available from both eyes of a subject, the eye with the worse visual acuity was used. All locations with a zero sensitivity and their immediate neighbors were not included in this analysis to avoid artefactual reduction of variability that may occur in regions with severe vision loss as a result of the "floor effect," whereby data are forced to the lowest number (i.e., highest light intensity) available by the instrument. Coincidentally, the test–retest limit calculated in patients with *RPE65*-LCA was similar to the limit (i.e., 3 SD) of interindividual variability (0.72 log units) observed in normal subjects.

In retinal regions with evident biological activity, dark adaptation testing was performed to define the rod and cone visual cycle kinetics (12–19). A yellow full field–adapting light exposure of 7 log scot-td·s was delivered with a flash unit mounted at the top of a 150-mm-diameter sphere with a white inner coating and an opening for the subject's eye. In a fully dark-adapted healthy eye, ≈60% of the available rhodopsin molecules would be expected to absorb a primary quantum with this flash. The adapting flash was delivered under near-infrared (NIR) viewing of the subject's pupil to avoid reduction in retinal exposure caused by partially closed eyelids. During testing, NIR LEDs illuminated the pupil and an NIR-sensitive camera allowed continuous monitoring of pupil position. The stimuli used were blue or red LEDs illuminating an opal diffuser (1.7° diameter); for testing healthy eyes, a three–log unit neutral density filter was intercalated between the blue LED and the diffuser to shift the whole dynamic range of the instrument to lower illuminances. Under software control, LEDs were driven with amplitude and pulse-width modulation to achieve a 5.8 log unit dynamic range. Thresholds to blue and red stimuli were determined using a staircase procedure before and at regular intervals after the adapting flash. Differences between the sensitivities to blue and red stimuli were used to determine the type of photoreceptor mediating vision. Log-linear segments of rod-mediated recovery were fit with lines to estimate exponential time constants.

In addition, two-color perimetry (blue, 500 nm; red, 650 nm) was performed during the cone-plateau period following the adapting flash and/or under standard (1–2 h) and extended (3–8 h) dark adaptation conditions to understand the retinal distribution of cone- and rod-mediated vision across the treated areas. Patient 1 could not perceive the highest intensity available with the standard-sized chromatic stimuli. Therefore, larger (4° diameter) blue (500 nm), orange (600 nm), and red (650 nm) stimuli were used posttreatment to estimate type of photoreceptor mediation within his region of biological activity. Pretreatment, one of the patients (patient 2) could perceive chromatic stimuli only to eccentricities <3 mm; the other two patients could not perceive the stimuli at any extrafoveal locus. Thus, pretreatment cone- and rod-mediated vision was estimated from achromatic sensitivities using the most conservative assumption that both rods and cones were contributing to this very low level of vision.

Fixation Location and Stability Studies. Preferred retinal locus used by patients with *RPE65*-LCA to fixate to a stationary target and the stability of fixation were determined by video imaging of the retina under NIR light and recording the movement of each video image obtained at a 25-Hz rate with respect to a reference image (MP1; Nidek Technologies America). Recordings were

monocular (eyes were tested sequentially) and performed during a fixation task involving visualization of a red target; the total length of recording was 45 seconds. The fixation light was ≈3 log units brighter than normal perceptual threshold, and all patients tested could see the target throughout the recording period. The movement of the retinal image with respect to the fovea was recorded as horizontal and vertical offset values as a function of time. A representative 10-s epoch was selected; horizontal and vertical offsets were converted to radial distances and the SD of these radial distances over the 10-s epoch was reported as a measure of fixation instability (2).

Pupillometry Studies. The direct transient pupillary light reflex (TPLR) was elicited and recorded (20, 21). TPLR luminance-response functions were derived from responses to increasing intensities (from −6.6 to 2.3 log scot-cd·m^{-2}) of green stimuli with short duration (0.1 s) presented monocularly in the dark-adapted state. The light stimulated pupil was imaged with an infrared-sensitive video camera (LCL-903HS; Watec America) and images were digitized by two instruments simultaneously. A digital image processor (RK-706PCI, ver. 3.55; Iscan) sampled the horizontal pupil diameter at 60 Hz and a video digitizer (PIXCI SV4 board, ver. 2.1; Epix) produced a computer file of the video sequence. Records were 5.7 s long, with a 1-s pre-stimulus baseline. TPLR amplitude was defined as the difference between the pupil diameter at a fixed time (0.9 s) after the onset of the stimulus and the pre-stimulus baseline. TPLR response threshold was defined as the stimulus luminance that evoked a criterion (0.3 mm, limit of spontaneous oscillations in pupil diameter, ref. 20) contraction of the pupil diameter at the fixed time (0.9 s) considered.

Animal Studies. Naturally occurring *Rpe65*-mutant *rd12* mice (n = 20) were used. Procedures were conducted in accordance with the ARVO Statement for the Use of Animals in Ophthalmic and Visual Research and with institutional approval. Breeding, origins, maintenance before and after surgery, and surgical details have been described (22, 23). In the first set of experiments, a single 1-μl subretinal injection of the rAAV2-CB^{SB}-h*RPE65* vector, which remained in the syringe after each human surgery, was delivered subretinally to one eye of *rd12* mice (ages 17–52 d). The non-injected eyes of the same animals served as controls. ERG recordings were performed 25 to 37 days after the injection. In a second set of experiments, *rd12* mice were used to study early effects of uniocular subretinal injection of rAAV2-CB^{SB}-h*RPE65* vector (n = 2) and of BSS vehicle (n = 2). Non-injected eyes of the same animals served as controls. ERG recordings were performed at 10 days after the injections. In both experiments, full field bilateral ERGs were recorded as described (23). Animals were dark-adapted (>12 h) and anesthetized with intramuscular ketamine HCl (65 mg/kg) and xylazine (5 mg/kg); corneas were anesthetized with proparacaine HCl, and pupils dilated with tropicamide (1%) and phenylephrine (2.5%). Responses evoked by a 0.1 log scot-cd·s·m^{-2} flash were amplified, filtered (−3 dB cutoff at 0.3 and 300 Hz) and digitized (2 kHz) with a 12-bit analog-to-digital converter. B-wave amplitudes were measured conventionally, from baseline or a-wave trough to positive peak, and vector-injected eyes were plotted against non-injected fellow eyes. Existence of a significant efficacy resulting from vector was defined in each animal by comparison to the expected variability (i.e., 3 SD) of interocular differences of this waveform amplitude in untreated *rd12* and WT eyes (23). To test for the possibility that preformed RPE65 protein—either contained within the vector capsid or adhering to its surface—was responsible for the rapid therapeutic response seen in these mice, we performed an hRPE65 ELISA on 10 μl of undiluted test vector (1.4×10^{13} vector genomes per ml) diluted in 90 μl of coating buffer containing 2% SDS, then boiled for 5 min before coating the ELISA plate. For the positive control, ELISA wells were coated with 0.5 μg/well hRPE65 protein expressed from *Escherichia coli* and pretreated as for the test vector. Anti-RPE65 monoclonal antibody (1 mg/ml) (Chemicon, cat# MAB 5428) at a dilution of 1:640,000 was used to detect hRPE65 in all wells and to generate the highest point in a standard curve. No hRPE65 was detected in clinical vector samples or in similar preclinical vector within the limits of the assay (data not shown), suggesting that expression from the hRPE65 transgene after delivery to the RPE by vector most likely accounts for the rapid therapeutic response.

1. Jacobson SG, *et al.* (2005) Identifying photoreceptors in blind eyes caused by RPE65 mutations: prerequisite for human gene therapy success. *Proc Natl Acad Sci USA* 102:6177–6182.
2. Jacobson SG, *et al.* (2007) Human cone photoreceptor dependence on RPE65 isomerase. *Proc Natl Acad Sci USA* 104:15123–15128.
3. Aleman TS, *et al.* (2007) Inner retinal abnormalities in X-linked retinitis pigmentosa with RPGR mutations. *Invest Ophthalmol Vis Sci* 48:4759–4765.
4. Aleman TS, *et al.* (2008) Retinal laminar architecture in human retinitis pigmentosa caused by rhodopsin gene mutations. *Invest Ophthalmol Vis Sci* 49:1580–1590.
5. Cideciyan AV, *et al.* (2007) Centrosomal-ciliary gene CEP290/NPHP6 mutations result in blindness with unexpected sparing of photoreceptors and visual brain: implications for therapy of Leber congenital amaurosis. *Hum Mutat* 28:1074–1083.
6. Jacobson SG, *et al.* (2008) Photoreceptor layer topography in children with Leber congenital amaurosis caused by *RPE65* mutations. *Invest Ophthalmol Vis Sci*, in print
7. Huang Y, *et al.* (1998) Relation of optical coherence tomography to microanatomy in normal and rd chickens. *Invest Ophthalmol Vis Sci* 39:2405–2416.
8. Jacobson SG, *et al.* (1986) Automated light- and dark-adapted perimetry for evaluating retinitis pigmentosa. *Ophthalmology* 93:1604–1611.
9. Jacobson SG, Yagasaki K, Feuer W, Roman AJ (1989) Interocular asymmetry of visual function in heterozygotes of X-linked retinitis pigmentosa. *Exp Eye Res* 48:670–691.
10. Van Hooser JP, *et al.* (2000) Rapid restoration of visual pigment and function with oral retinoid in a mouse model of childhood blindness. *Proc Natl Acad Sci USA* 97:8623–8628.
11. Jacobson SG, *et al. (2007) RDH12* and. *RPE65*, visual cycle genes causing Leber congenital amaurosis, differ in disease expression *Invest Ophthalmol Vis Sci* 48:332–338.
12. Jacobson SG, *et al.* (1995) Night blindness in Sorsby's fundus dystrophy reversed by vitamin A. *Nat Genet* 11:27–32.
13. Cideciyan AV, Pugh EN Jr, Lamb TD, Huang Y, Jacobson SG (1997) Rod plateaux during dark adaptation in Sorsby's fundus dystrophy and vitamin A deficiency. *Invest Ophthalmol Vis Sci* 38:1786–1794.
14. Cideciyan AV, *et al.* (1998) Null mutation in the rhodopsin kinase gene slows recovery kinetics of rod and cone phototransduction in man. *Proc Natl Acad Sci USA* 95:328–333.
15. Cideciyan AV, *et al.* (1998) Disease sequence from mutant rhodopsin allele to rod and cone photoreceptor degeneration in man. *Proc Natl Acad Sci USA* 95:7103–7108.
16. Cideciyan AV, *et al.* (2000) Rod and cone visual cycle consequences of a null mutation in the 11-cis-retinol dehydrogenase gene in man. *Vis Neurosci* 17:667–678.
17. Poehner WJ, *et al.* (2000) A homozygous deletion in RPE65 in a small Sardinian family with autosomal recessive retinal dystrophy. *Mol Vis* 6:192–198.
18. Jacobson SG, Cideciyan AV, Wright E, Wright AF (2001) Phenotypic marker for early disease detection in dominant late-onset retinal degeneration. *Invest Ophthalmol Vis Sci* 42:1882–1890.
19. Cideciyan AV, *et al.* (2004) Mutations in ABCA4 result in accumulation of lipofuscin before slowing of the retinoid cycle: a reappraisal of the human disease sequence. *Hum Mol Genet* 13:525–534.
20. Aleman TS, *et al.* (2004) Impairment of the transient pupillary light reflex in Rpe65-/- mice and humans with Leber congenital amaurosis. *Invest Ophthalmol Vis Sci* 45:1259–1271.
21. Aguirre GK, *et al.* (2007) Canine and human visual cortex intact and responsive despite early retinal blindness from RPE65 mutation. *PLoS Med* 4:e230.
22. Pang JJ, *et al.* (2005) Retinal degeneration 12 (rd12): a new, spontaneously arising mouse model for human Leber congenital amaurosis (LCA). *Mol Vis* 11:152–162.
23. Roman AJ, *et al.* (2007) Electroretinographic analyses of Rpe65-mutant rd12 mice: developing an in vivo bioassay for human gene therapy trials of Leber congenital amaurosis. *Mol Vis* 13:1701–1710.

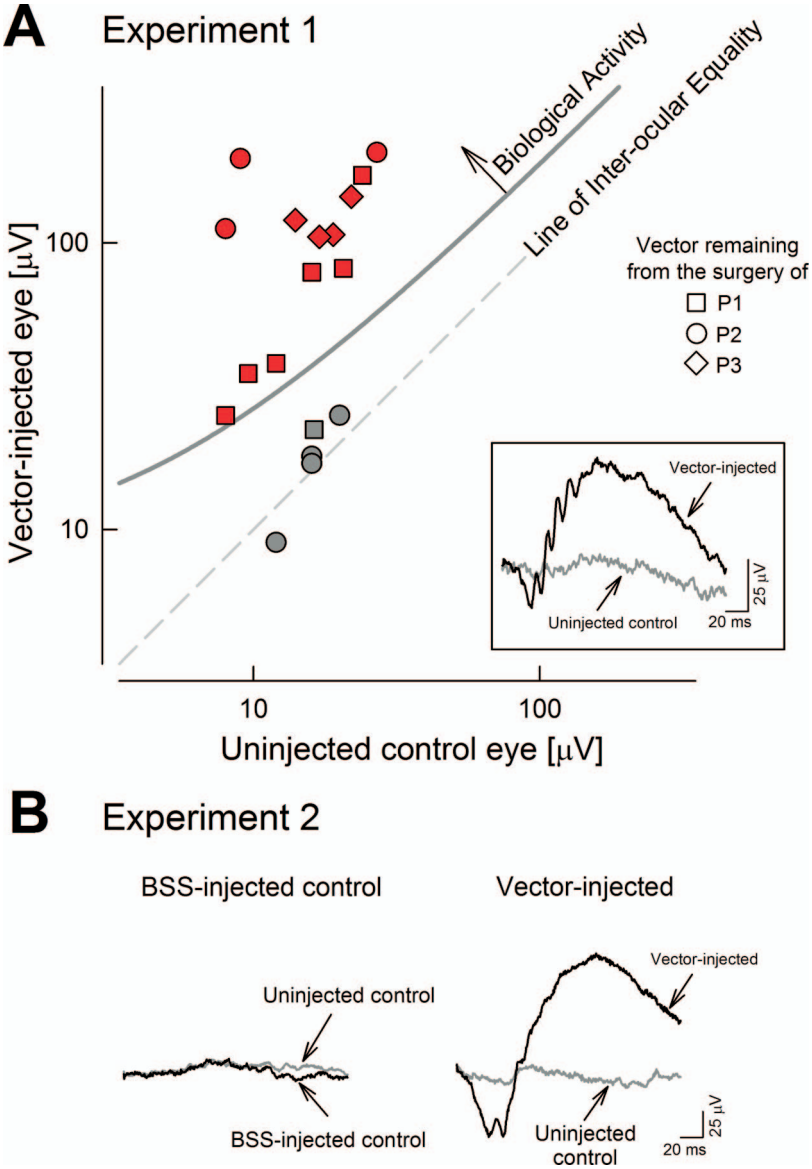

Fig. S1. Hypothesis testing regarding human results after treatment using the *rd12* mouse model of Rpe65 deficiency. (*A*) In experiment 1, *in vivo* bioassay of the gene therapy vector used in human surgery shows biological activity. Electroretinographic (ERG) b-wave amplitudes in vector-injected eyes versus non-injected control eyes of *rd12* mice. Vector (1 μl) is from the syringe used in the surgery of each *RPE65*-LCA subject (patient 1, squares; patient 2, circles; patient 3, diamonds). Dashed line of equality corresponds to no interocular difference in this ERG parameter. Solid line defines upper limit of significant interocular difference (3 SD) derived from untreated *rd12* and WT animals. Thirteen treated eyes (red symbols) showed a significant ERG improvement in the treated eyes, whereas five (gray symbols) did not. Significant ERG improvements provide evidence of the biologic activity of the vector used for each patient; small subset of failures are attributed to the surgical uncertainty of delivering vector unerringly to the subretinal space in the small mouse eye. (*Inset*) ERG waveform from a vector-injected (black trace) versus the non-injected control eye (gray trace) of an *rd12* mouse from this experiment. (*B*) In experiment 2, robust biological activity is observable as early as 10 days after injection. Representative ERG waveforms 10 days after subretinal injection of vector (*Right*; black traces) or vehicle (*Left*; black traces) compared with non-injected control eyes (gray traces). These results suggest that surgical detachment of the retina with a subretinal injection not containing vector does not cause an ERG improvement.

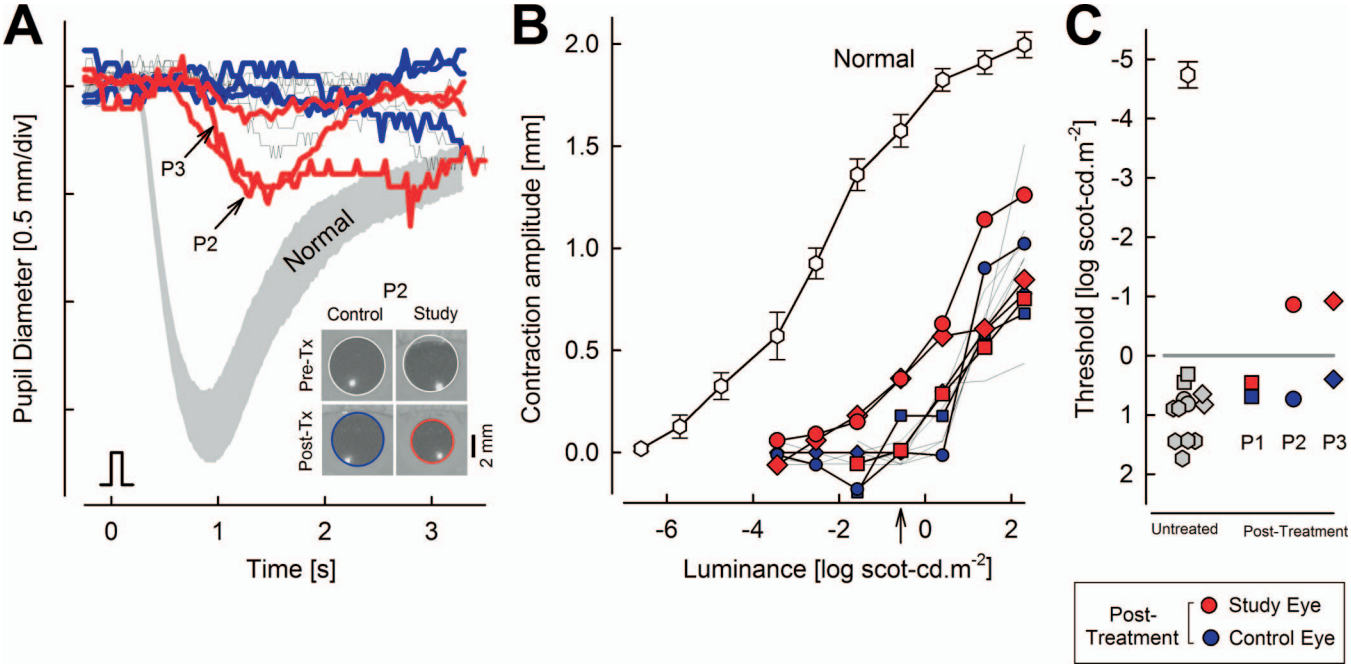

Fig. S2. Pupillary responsivity increases after treatment. (*A*) Change in pupil diameter evoked by a short duration light stimulus (0.1 s, −0.6 log scot-cd·m^{-2}, green, dark-adapted) in study and control eyes of the three patients at 18 months before treatment (thin black traces) and 1 month after treatment (red, study eye; blue, control eye) compared with results from normal subjects (gray band, mean ± 2 SEM; $n = 13$). Pretreatment eyes do not show changes in pupil diameter that are distinguishable in magnitude (<0.3 mm) from spontaneous oscillations of the pupil diameter of the dark-adapted eye. Posttreatment (red) traces show sizable pupil contractions in the study eyes of two of the patients (patients 2 and 3) but not in patient 1. Pupils from control eyes (blue traces) after treatment do not contract in response to this stimulus. Stimulus monitor trace at the bottom left. (*Inset*) Video frames of pupils of control and study eyes of patient 2 at 0.9 s after the light stimulus; pupillary margin is outlined in white (pretreatment), red (posttreatment, study eye), or blue (posttreatment, control eye) for visibility; calibration bar at the bottom right. (*B*) Luminance response functions measured at 0.9 s after stimulus onset in both eyes of each patient before treatment (thin black lines) and after treatment in the study eye (red) compared with the control eye (blue) and with normal data (mean ± SEM, white symbols). Before treatment (thin black lines), pupil contractions were observed only with the two highest luminance stimuli. After treatment (red symbols), there were contractions in the study eye of patients 2 and 3 within a range of stimuli and there was a shift of the luminance response function to the left; no such responding was recorded in patient 1 or in the control eyes. Arrow points to stimulus luminance of the waveforms shown in *A*. (*C*) Pupillary response thresholds in patients with untreated *RPE65*-LCA (gray hexagons, other *RPE65*-LCA patients; gray squares, patient 1; gray circles, patient 2; gray diamonds, patient 3) show abnormalities in excess of 5 log units compared with normal (white hexagon, mean ± 2 SD). Thresholds in the study subjects before treatment are similar to each other and to other patients with *RPE65*-LCA (gray hexagons, $n = 3$; gray line, mean ± 2 SD for untreated *RPE65*-LCA). The treated eye of patient 2 improved by 1.6 log units, from 0.74 log scot-cd·m^{-2} before treatment to −0.86 log scot-cd·m^{-2} after treatment (red). Patient 3 improved by 1.8 log units from 0.83 log scot-cd·m^{-2} before treatment to −0.92 log scot-cd·m^{-2} after treatment. The untreated eyes did not change (blue symbols). Patient 1 showed no detectable changes, which may be attributed to the smaller increase in posttreatment visual sensitivity compared with patients 2 and 3.

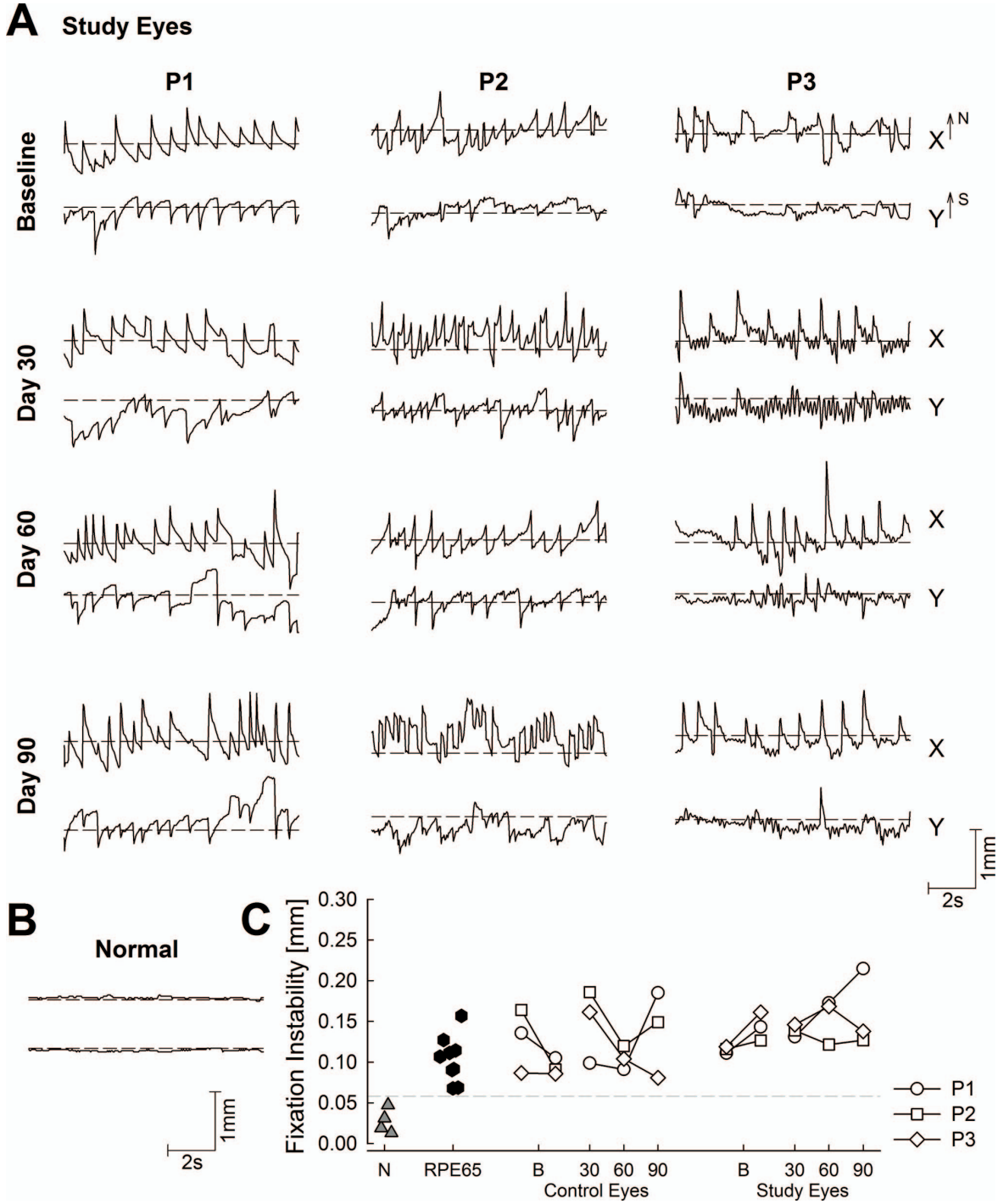

Fig. S3. Fixation location and fixation stability of control and study eyes do not change after treatment. (*A*) Pairs of traces show the x- and y-axis deflections of the location of the fovea recorded with infrared fundus imaging over 10-s epochs in the study eyes of three patients at baseline and days 30, 60, and 90 after treatment. Control eyes showed similar results (not shown). Horizontal dashed lines are the reference location of the fovea at the start of the recording session 15–35 s preceding the selected epoch. All patients show abnormal eye movements with horizontal and vertical components of instability and larger amplitude jerk nystagmus occurring at frequencies of ≈1–2 Hz. All plots are shown as equivalent left eyes for clarity and consistency with other figures. (*B*) Traces from a representative normal subject. (*C*) Summary of fixation instability in all subjects. Horizontal dashed line is a conservative (+3 SD) upper limit of normal (N) from the mean value. Study and control eyes of patients 1, 2, and 3 at two baseline (B) visits show fixation instability similar to other patients with *RPE65*-LCA (dark hexagons). At posttreatment days 30, 60, and 90, there are no consistent increases or decreases in fixation instability for the study and control eyes.